Tuning the emission characteristics of top-emitting organic light-emitting devices by means of a dielectric capping layer: An experimental and theoretical study

H. Riel,[a] S. Karg, T. Beierlein, and W. Rieß
IBM Research, Zurich Research Laboratory, 8803 Rüschlikon, Switzerland

K. Neyts
University of Ghent, St. Pietersnieuwstraat 41, 9000 Ghent, Belgium

(Received 17 March 2003; accepted 9 July 2003)

The emission characteristics of top-emitting organic light-emitting devices (OLEDs) have been studied experimentally and theoretically to derive a quantitative understanding of the effect of a dielectric capping layer. We demonstrated that the angular intensity distribution and the spectral characteristics can be tuned and the light outcoupling enhanced simply by varying the optical thickness of a dielectric layer deposited on top of a semitransparent metal electrode. With the capping-layer concept, the outcoupled light intensity in forward direction was increased by a factor of 1.7, and concomitantly a high color purity achieved. An optical model based on a classical approach was used to calculate the emission characteristics. The excellent agreement between measured and simulated data shows that the capping layer controls the interplay between different interference effects such as wide-angle and multiple-beam interference occurring in top-emitting OLEDs. The strength of the capping layer concept is in particular that the optical and the electrical device performance can be optimized separately. © *2003 American Institute of Physics.*
[DOI: 10.1063/1.1605256]

I. INTRODUCTION

In recent years, major breakthroughs have led to significant improvements in the performance of organic light-emitting devices (OLEDs).[1–4] For example, by improving the charge-carrier balance[2,5,6] and using emitting materials with high fluorescence efficiency[1,7] and, more recently, phosphorescent emitters,[3,8,9] the internal quantum efficiency of optimized OLEDs is gradually being moved closer to its theoretical limits. Therefore, further improvements of the external quantum and the power efficiency can only be expected from an increase of the outcoupling efficiency.[10,11] More recently, the optical design has attracted considerable attention as a means of tailoring the emission properties of OLEDs. It has been found that the external quantum efficiency as well as the spectral characteristic significantly depend on the OLED architecture, in particular on the layer thicknesses, owing to optical interference effects.[12–14] Fukuda and co-workers demonstrated that a change of the thickness of the hole-transporting layer (HTL) as well as of the transparent indium–tin–oxide anode in bottom-emitting OLEDs leads to a shift of the electroluminescence (EL) spectrum and a variation of the EL intensity by a factor of 2 in the material set used.[13] The influence of the electron-transport-layer (ETL) thickness on the optical properties of bottom-emitting devices was studied by So and co-workers.[12] They explained their results by wide-angle interference [see Fig. 1(a)] arising from the superposition of the amplitudes of direct emission and emission reflected from the cathode mirror. In top-emitting devices, where EL is outcoupled through a semitransparent thin metal cathode with transmittance $T \geqslant 0.35$ as used in this article, the influence of interference effects is even stronger. In this case, both wide-angle and multiple-beam interference (see Fig. 1) have to be taken into account.[15] Consequently, in top-emitting OLEDs the strength of the optical interference effects depends critically on the reflectivity of the metal cathode, and accordingly, controlling the cathode reflectivity is a further degree of freedom in tailoring the emission characteristics. The thickness variation of the cathode metal is one possibility to change the reflectivity. However, this approach has the disadvantage of increasing absorption losses for thicker metal layers and of insufficient conductivity for a thinner metal cathode. A preferred concept, known from the optics of metal coatings, utilizes a thin dielectric layer on top of a thin metal film to modulate the transmittance of the cathode.[16] This approach was recently applied to top-emitting OLEDs by Hung and co-workers.[17] They demonstrated that by using an organic layer on top of a thin metal cathode a significant improvement in light output can be achieved because of the enhancement of optical transmission, and concluded that optimum performance is achieved at the highest cathode transparency.

In this article we present a joint experimental and theoretical analysis of the EL emission pattern of top-emitting multilayer OLEDs. A dielectric capping layer was applied on top of a thin metal cathode to tune the emission characteristics and to enhance light outcoupling. The wide-band-gap semiconductor ZnSe with a refractive index of $n = 2.6$ was used as capping material. Detailed investigations of the in-

[a]Author to whom correspondence should be addressed; electronic mail: hei@zurich.ibm.com

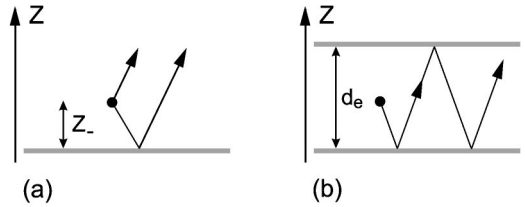

FIG. 1. Illustration of (a) wide-angle and (b) multiple-beam interference. z_- denotes the distance between the light-emitting molecule and the mirror with the higher reflectivity. d_e is the total distance between the two electrodes.

fluence of the capping-layer thickness on the efficiency, the emission pattern and the spectral characteristics as a function of the viewing angle are presented and compared with simulation results. The optical effects induced by the dielectric capping layer are explained by means of an optical model. The optical model uses a classical approach based on the equivalence between the probability for the emission of a photon by a dipole transition and the power radiated by a classical elementary dipole antenna.[18] It is demonstrated that the light emission is not maximum at highest transmittance of the cathode but that rather it is determined by an interplay between the different interference effects, which are governed by the thickness of the capping layer.

II. DEVICE PREPARATION AND EXPERIMENTAL METHODS

The devices are built on glass substrates (Schott AF45) precoated with a highly reflective bilayer anode consisting of Al covered with a thin Ni layer as hole-injecting anode.[19] The organic multilayer structure consists of copper phthalocyanine (CuPc) as buffer layer, N,N′-di(naphthalene-1-yl)-N,N′-diphenyl-benzidine (NPB) as HTL, 4,4′-N,N′-dicarbazole-1,1′-biphenyl (CBP) doped with 6% tris(2-phenylpyridine)iridium ($Ir(ppy)_3$) as emission layer, 2,9-dimethyl-4,7-diphenyl 1,10-phenanthrolin (BCP) as hole-blocking layer, and tris(8-hydroxyquinolinato)aluminum (Alq_3) as ETL (see Fig. 2). The organic-layer thicknesses were optimized with the combinatorial method to be 20 nm CuPc, 40 nm NPB, 20 nm CBP doped with 6% $Ir(ppy)_3$, 10 nm BCP, and 40 nm Alq_3.[14,20] In the top-emitting device architecture used, sketched in Fig. 2, EL is observed through a semitransparent metal cathode consisting of 12 nm Ca and 12 nm Mg. In further steps the multilayer structure was capped with a ZnSe layer to adjust the transmittance of the metal cathode.[21] The active area of the devices investigated was $2\times3\ mm^2$.

The organic materials were purified by vacuum sublimation. Depositions were carried out in a high vacuum system at a chamber base pressure ranging between 4×10^{-7} and 1×10^{-6} mbar by thermal evaporation from resistively heated boats. Typical deposition rates for the organic compounds, the metal and ZnSe were ≈1 Å/s and, accordingly, 0.06 Å/s for the dopant. Calibrated quartz-crystal monitors were used to control the deposition rates individually. Characterization of the OLED was performed under inert conditions in a glove-box system filled with Ar and directly connected to the deposition chamber. Current–voltage ($I-V$) and EL–V characteristics were measured with a Hewlett Packard parameter analyzer (HP 4145B) and a sensitive Si photodiode (Hamamatsu S2281) capturing light emitted into a viewing angle of $\pm40°$. The spectral characterization and the luminance calibration of the photodiode were performed with a Photo Research PR704 spectroradiometer. To investigate the angular dependence of the spectral characteristics and the intensity distribution, the OLED was mounted on a rotary stage, which enabled the surface normal vector of the device to be tilted with respect to the optical axis. The emission spectrum and the EL intensity of the device were measured with the Photo Research PR704 spectroradiometer under constant-current condition at various emission angles. To ensure that the measurement spot of the spectroradiometer always remained smaller than the active area of the OLED visible under a certain angle, the 0.125° aperture was used. Under these conditions accurate angular measurements up to $\approx\pm80°$ are possible.

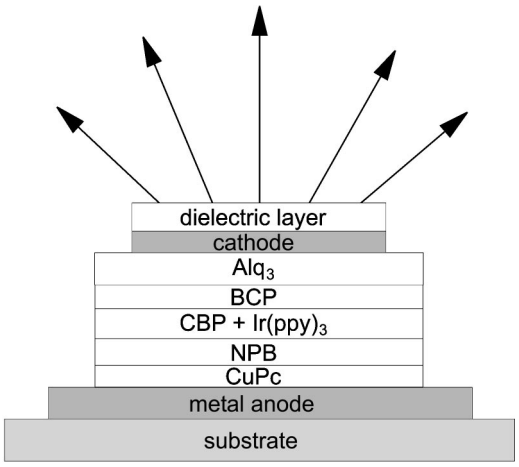

FIG. 2. Schematic diagram of the planar top-emitting device structure studied. A dielectric capping layer is applied on top of the semitransparent metal cathode to tune the emission characteristics. The organic-layer thicknesses are 20 nm CuPc, 40 nm NPB, 20 nm CBP doped with 6% $Ir(ppy)_3$, 10 nm BCP, and 40 nm Alq_3.

III. OPTICAL MODEL

An accurate model for light emission from the OLED device has to take into account partial reflections at interfaces and the resulting interference effects. The optical model we used has been described in several articles[18,22,23] and is based on the equivalence between the emission of a photon due to an electrical dipole transition and the radiation from an electrical dipole antenna. It is assumed that the emitting layer contains a large number of mutually incoherent dipole radiators with arbitrary orientation.

Emission from the electrical dipole radiator towards the bottom is reflected by the mirror and interferes with the emission towards the top. The resulting wide-angle interference effects depend on the orientation of the dipole, the polarization of the light [transversal electric (TE) or transversal magnetic (TM)] and the distance between emitter and mirror. Our structure has a metallic top electrode with considerable

reflectivity. Therefore light can reflect back and forth between the two mirrors, leading to multiple-beam interferences in the emitted light. The multiple-beam interference factor depends on the angle of the emission, the polarization of the light and the distance between the two mirrors. These two interference effects that occur in the optical microcavity structure are illustrated in Fig. 1. The total emission from the OLED is obtained by averaging the emission over all possible dipole orientations (with random distribution) and locations (the dipoles are assumed to be homogeneously distributed in the 20-nm-thick CBP layer) of the dipole emitters.

The equivalence between the radiating dipole antenna and the molecular dipole transition requires that the probability for spontaneous emission of a photon (dipole transition) is proportional to the integrated dipole antenna radiation. If the excited state of the organic molecule is located in a microcavity, which increases the probability for spontaneous emission, the radiative decay time will be reduced accordingly. In planar microcavities where the excited organic molecules or polymer chains are at a distance of several tens of nanometers from the metallic layers, the modulation of the decay time is rather small. In this article we have neglected the small effect of the change in radiative decay rate of the excited state in the simulation of the emission characteristics.

Other ways of modeling the emission from a planar optical structure have been proposed. One method that is often used determines the coupling between the dipole emitter and the local density of photon states.[24–26] This method only leads to the same result as the method described above if there is no absorption in the layer stack. However, as mentioned in Refs. 18 and 27, absorbing layers cannot be taken into account with the method based on the density of states. In the structure discussed here two metal electrodes are present, and one of them is semitransparent. It is therefore essential to take the losses in the metal films into account.

A simulation program described elsewhere[15,18] is used for calculating the angle and wavelength dependence of the emission from the different OLED structures into air, through the metallic top electrode. The simulation program requires the following input parameters: thickness and complex refractive index for every layer in the structure, position and width of the recombination zone, and the unperturbed emission spectrum without interference effects present. For the organic materials the complex refractive indices were obtained by ellipsometer measurements, and we used data from the literature for the values of the metals and ZnSe.[28] The photoluminescence (PL) spectrum of the $Ir(ppy)_3$ complex in solution was used as intrinsic spectral distribution of the emitter.

IV. RESULTS AND DISCUSSION

The main goal of this article is the quantitative understanding of the effect a dielectric capping layer on top of a semitransparent metal cathode has on the OLED performance. Therefore, the EL emission characteristics were investigated experimentally and theoretically as a function of the ZnSe thickness. ZnSe was deposited on top of the Ca/Mg cathode of a phosphorescent OLED. The thickness of the dielectric capping layer was sequentially increased from 0 to 110 nm on the same OLED. After each ZnSe growth sequence, electrical and optical measurements were performed under inert conditions. Figure 3 shows the efficiency of the phosphorescent top-emitting OLED as a function of the current density for various ZnSe layer thicknesses. A significant influence of the ZnSe thickness on the outcoupled EL intensity can be observed. An efficiency of 38 cd/A at 10 μA/cm^2 was achieved already without capping layer, owing to the efficient phosphorescent device structure and the highly reflective anode. The efficiency increased to a maximum value of 64 cd/A when using a 60-nm-thick ZnSe capping layer. Note that the general functional behavior of the efficiency curves and also the $I-V$ characteristics[21] are not influenced by the deposition of the dielectric layer. This indicates that the electrical properties of the OLED, including the charge balance factor, are not affected by the capping layer. The EL efficiency enhancement of a factor of 1.7 is therefore purely due to the modified optical architecture. In other words, the number of generated excitons in the OLED is identical; however, the number of photons detected externally in the solid angle considered is significantly affected by a modification of the optical structure.

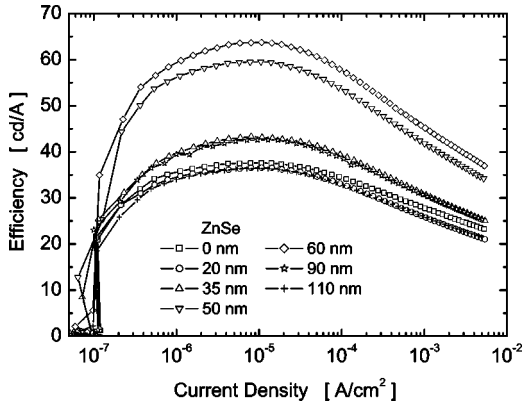

FIG. 3. Efficiency (cd/A) vs current density of the OLED for various capping-layer thicknesses. OLED structure: Al / Ni / 20 nm CuPc / 40 nm NPB / 20 nm CBP doped with 6% $Ir(ppy)_3$ / 10 nm BCP / 40 nm Alq_3 / 12 nm Ca / 12 nm Mg / X nm ZnSe.

In Ref. 21 it was demonstrated that the transmittance of the Ca/Mg/ZnSe layer sequence changes periodically with the ZnSe thickness. The transmittance of the uncovered cathode consisting of 12 nm Ca and 12 nm Mg is about 0.52. With increasing capping-layer thickness, it reaches a maximum of 0.78 at about 20 nm and a minimum of 0.32 at about 65 nm ZnSe. The experimentally found thickness of 60 nm ZnSe for maximum efficiency therefore does not coincide with the value of 20 nm for the highest transmittance of the cathode configuration, but matches well with the value at which minimum transmittance occurs. This discrepancy substantiates the fact that the simple assumption that maximum outcoupling is obtained at maximum transmittance of one electrode, here the cathode, is not valid. The correlation between the two parameters is much more complex. To explain the experimental results qualitatively and also quantitatively, interference effects present in structures of this type have to be taken into consideration. The optical model described in

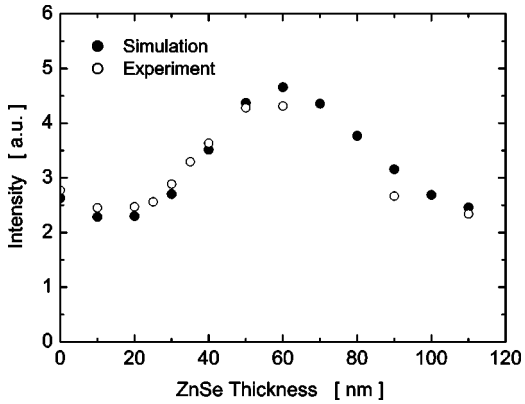

FIG. 4. Simulated (solid circles) and measured (open circles) EL intensity (radiometric) emitted in forward direction as a function of ZnSe thickness. The simulated values are scaled by the same constant factor for an optimum fit to all measurements. The measurements were performed under constant-current conditions using 12.5 mA/cm^2.

Sec. III inherently takes into account wide-angle as well as multiple-beam interference (see Fig. 1) and is thus ideally suited to calculate the emission characteristics of planar, top-emitting OLEDs. In the following, an extensive dataset comprising not only the EL intensity distribution as a function of the ZnSe thickness but also the spectral characteristics at different viewing angles and for different ZnSe thicknesses is presented and compared with the theoretical model. In particular, the experimental dataset allows a precise verification of the applicability of the optical model.

In Fig. 4 the dependence of the EL intensity emitted in forward direction on the ZnSe thickness is shown together with the corresponding simulated values. The simulated data were scaled by the same constant factor for an optimum fit to the measurements. This scaling is necessary because the simulation of the emission characteristics is based on a purely optical model that neglects electrical effects. To calculate absolute numbers for the outcoupled EL power would require that also the electrical properties of the device, such as the charge carrier balance and the singlet–triplet ratio, be taken into account. With increasing ZnSe thickness the outcoupled EL intensity first decreases slightly, exhibits a minimum between 10 and 20 nm, and finally reaches a maximum at 60 nm. For thicker ZnSe, the intensity falls off again, and for 110 nm ZnSe a value even lower than the one without capping is obtained. The data simulated by the optical model are in excellent agreement with the measurement presented here. This shows that interference effects within the device are responsible for the oscillatory behavior of the EL intensity emitted in forward direction. Furthermore, it substantiates that for an optimization of the outcoupled light it does not suffice to consider only the transparency of the cathode.

The interplay between the different interference effects directly affects the outcoupled intensity and also influences the spectral characteristics significantly. Figure 5(a) depicts a set of normalized EL spectra for selected ZnSe thicknesses. The spectral weight of the EL emission shifts strongly when the capping-layer thickness is varied. Without ZnSe, the EL intensity shows a maximum at 512 nm and a full width at half maximum (FWHM) of 72 nm. A comparison with the

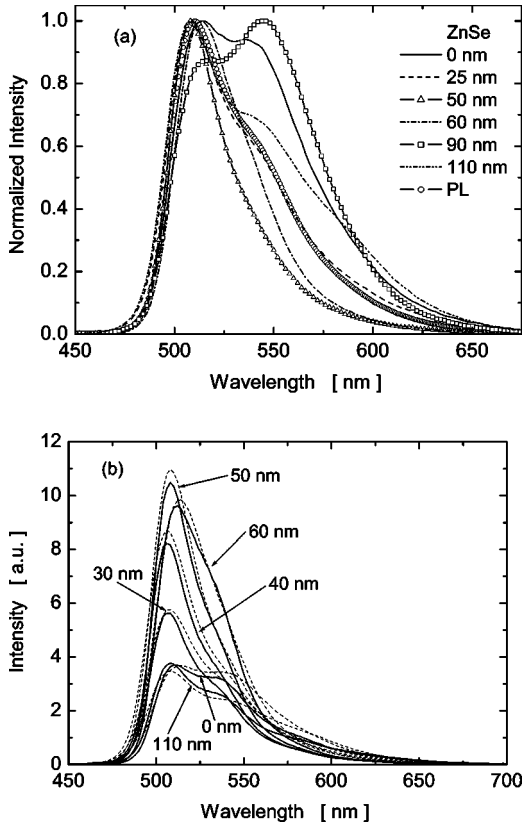

FIG. 5. (a) Normalized EL spectra measured at constant current density for various ZnSe thicknesses of the OLED shown in Fig. 2 ($I = 1.67$ mA/cm^2). The PL spectrum of Ir(ppy)$_3$ doped in CBP is shown as reference. (b) Comparison of the simulated (solid lines) and experimentally measured (dashed lines) spectral characteristics for ZnSe thicknesses of 0, 30, 40, 50, 60, and 110 nm. The simulated spectra are all scaled by the same constant factor for an optimum fit to the experimental data.

PL spectrum of a thin-film reference sample of CBP doped with 6% of Ir(ppy)$_3$ reveals that the emitted EL spectrum of the uncapped OLED is modified already by the weak microcavity structure in which Al/Ni and Ca/Mg:Ag are used as highly and partially reflective electrode, respectively. The corresponding EL spectrum exhibits a second peak at 536 nm, whereas the PL spectrum only shows a weak shoulder [see Fig. 5(a)]. The best agreement between EL and PL spectra is found for 25 nm ZnSe, where the cathode transmittance is very close to its maximum value.[21] With 50 nm ZnSe, a pure green emission with a peak at 508 nm and an extremely narrow FWHM of only 36 nm is observed, resulting in CIE 1931 color coordinates of $x = 0.19$ and $y = 0.67$. By further increasing the thickness of the dielectric layer, the spectrum broadens again, accompanied by a shift of the peak wavelength to 544 nm at 90 nm ZnSe thickness. At 110 nm ZnSe, the peak wavelength has moved back to 508 nm. In Fig. 5(b) the simulated spectral characteristics (solid lines) for six different ZnSe thicknesses and the corresponding EL intensities measured (dashed lines) are compared. The optical simulation excellently describes the dependence of the spectral characteristic on the ZnSe thickness. It is also remarkable that the calculated intensity ratios agree perfectly with the experiment. Note that all spectra are simulated with an identical set of optical input parameters. This provides strong

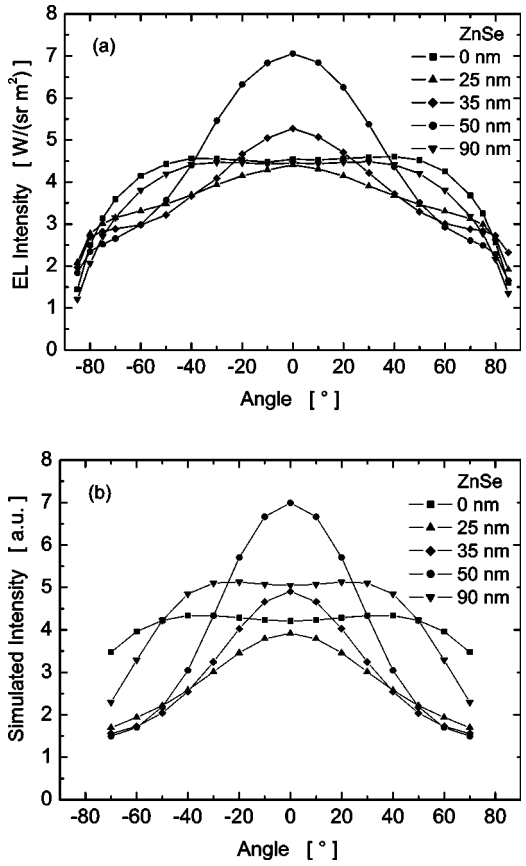

FIG. 6. (a) EL intensity in W/(sr m^2) as a function of the viewing angle of the OLED described with 0, 25, 35, 50, and 90 nm ZnSe as capping layer, measured at 12.5 mA/cm^2. (b) Corresponding simulated EL intensity.

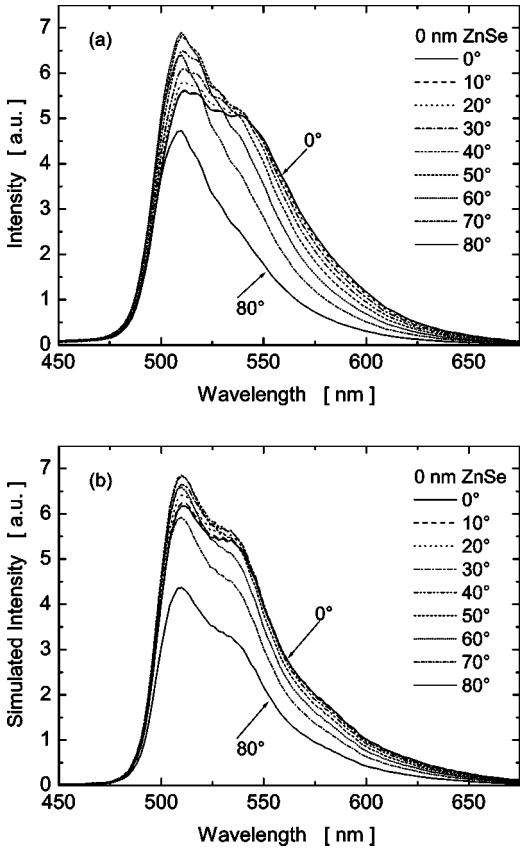

FIG. 7. (a) Measured and (b) simulated EL spectra for various viewing angles of the OLED shown in Fig. 2 without capping layer.

evidence that microcavity effects induced by a change of the cathode reflectivity caused by the capping layer are responsible for the spectral shift.

The spatial emission pattern strongly depends on the details of the optical architecture, in particular on the organic-layer thicknesses and the electrode reflectivity.[29] Hence, the comparison of experimental and simulated data provides a rigorous test of the validity of the optical model used. Figure 6(a) displays the EL intensity measured at 12.5 mA/cm^2 at selected ZnSe thicknesses as a function of the viewing angle. The emission pattern of the OLED without ZnSe is nearly Lambertian, and therefore has an almost constant intensity at all angles in this representation. With increasing ZnSe thickness, the externally detected EL intensity is enhanced in forward direction, and reduced for larger viewing angles. The most focussed emission pattern is found at a capping-layer thickness of 50 nm ZnSe, where an enhancement of the radiation by a factor of 1.6 is measured at 0° viewing angle. Under these conditions, also the integrated intensity (integration between $-70°$ and $+70°$) is increased, i.e., 110% compared with the case without capping. However, for 25 and 35 nm ZnSe, this integrated light output is reduced to 85% and 90%, respectively. By further increasing the ZnSe thickness, the spatial emission pattern returns to its original form, and at 90 nm almost corresponds to the one without capping. Even the integrated intensities are nearly identical. This behavior of the spatial emission pattern at different ZnSe thicknesses can be very well reproduced by the simulation. Figure 6(b) shows the simulated intensity as a function of the viewing angle. A comparison with the experimental data in Fig. 6(a) reveals that the shape as well as the intensity ratio are correctly described by the optical model. Only for larger viewing angles do we observe a slightly stronger decrease of the intensity in the simulation. However, the individual characteristics, such as the enhanced forward emission in the case of 50, 35, and 25 nm as well as the almost constant intensity distribution for the devices with 0 and 90 nm ZnSe, are evident.

From these results and theoretical and experimental investigations of microcavities,[15,30] it is expected that also the capping-layer thickness has a significant influence on the spectral characteristics measured at various viewing angles. It is demonstrated that for the various capping-layer thicknesses, the EL spectra exhibit a different functional dependence on the viewing angle. The spectral characteristics for the ZnSe thicknesses of 0, 35, and 50 nm measured at a current density of 12.5 mA/cm^2 at various viewing angles are presented in Figs. 7(a), 8(a), and 9(a). Without capping [Fig. 7(a)], the FWHM of the EL spectra decreases with larger viewing angle from 72 nm at 0° to 50 nm at 70°, whereas the peak wavelength stays almost constant at 510–512 nm. Up to a viewing angle of 40°, the spectra of the OLED without ZnSe still are very similar. Therefore the CIE 1931 color coordinates vary only slightly between 0.28 and 0.30 for the x coordinate and between 0.62 and 0.64 for the

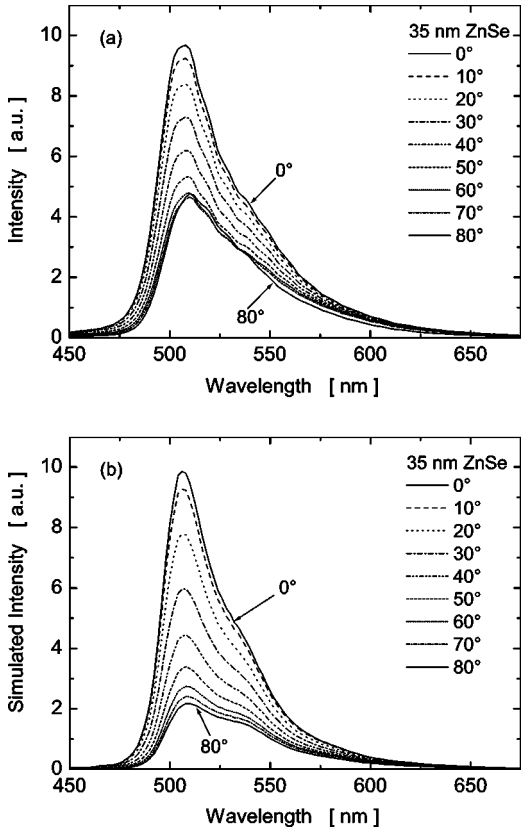

FIG. 8. (a) Measured and (b) simulated EL spectra for various viewing angles of the OLED shown in Fig. 2 with 35 nm ZnSe as capping layer.

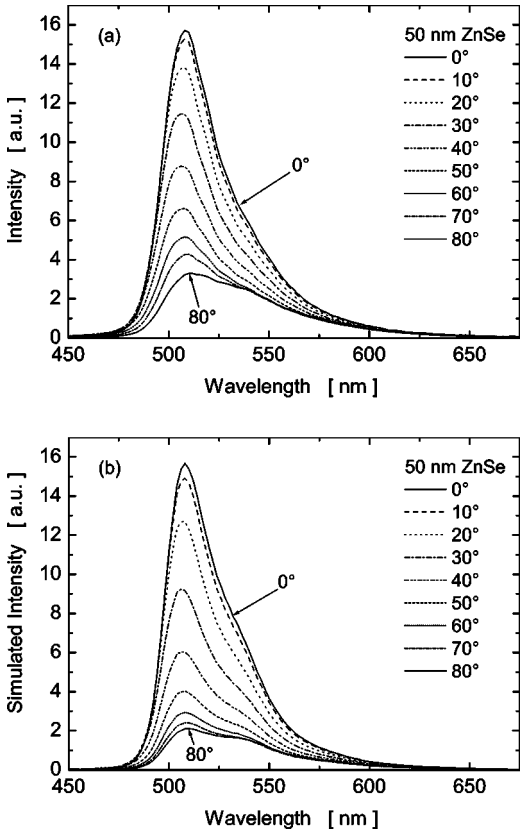

FIG. 9. (a) Measured and (b) simulated EL spectra for various viewing angles of the OLED shown in Fig. 2 with 50 nm ZnSe as capping layer.

y coordinate for a viewing angle between 0° and 40°.

At a ZnSe thickness of 35 nm the maximum as well as the width of the spectra are almost independent of the viewing angle [see Fig. 8(a)]. The EL intensities peak between 508 and 510 nm, and their FWHMs vary between 40 and 52 nm. Note that the color of EL emission of the OLED with 35 nm ZnSe appears quite pure because of the relatively narrow spectra. As a consequence the CIE 1931 color coordinates for viewing angles between $\pm 70°$ are $x = 0.23 \pm 0.01$ and $y = 0.63 \pm 0.01$.

Figure 9(a) shows the spectral characteristics of the OLED with 50 nm ZnSe on top measured at different angles. The decrease of emitted EL intensity with increasing viewing angle, which has already been observed in Fig. 6, is clearly visible. The corresponding peak wavelength is almost constant over the entire angular range. However, with increasing viewing angle, the EL intensity in the wavelength range at 550 nm is significantly enhanced compared with that in the region at 510 nm. This leads to a broadening of the spectral characteristic from 36 nm at 0° to 50 nm at 70°. The CIE 1931 color coordinates range from $x = 0.19$ and $y = 0.66$ for 0° to $x = 0.20$ and $y = 0.63$ for 40° viewing angle.

This shift of the spectral characteristic as a function of both viewing angle and capping-layer thickness can also be simulated by the optical model. The corresponding simulated spectra are shown in Figs. 7(b), 8(b), and 9(b) for 0, 35, and 50 nm ZnSe thickness, respectively. Again, these simulations agree very well with the experimental data. Only at larger viewing angles is a slightly stronger decrease in intensity observed for the calculated data. It is remarkable that the behavior of the peak wavelength and the changes in the FWHM are reproduced perfectly.

This extensive dataset demonstrates that the capping-layer thickness significantly influences the optical properties of the top-emitting OLED. As the device structure used represents a weak microcavity, wide-angle as well as multiple-beam interference occur, and it is their interplay that defines the optical properties and determines the emission characteristics of the OLED. By varying the capping-layer thickness the reflectivity of the top mirror and thus the interplay between wide-angle and multiple-beam interference can be controlled. As apparently neither of these effects predominates, both have to be taken into account. Consequently, the interpretation of the measured results is rather complex and, as demonstrated, a full calculation based on the interference of TE and TM emissions from parallel and orthogonal electrical dipoles is required. These aspects are explicitly taken into account in the optical model and the simulation program applied.

V. CONCLUSIONS

We have presented a comprehensive experimental and theoretical analysis that qualitatively and quantitatively explains the effect of a dielectric capping layer on the emission characteristics of top-emitting OLEDs. The extensive experimental dataset consisting of the EL intensity and the spectral characteristics as a function of viewing angle and capping-

layer thickness could be accurately simulated by using only a single set of optical-material input parameters. This is further proof of the versatility and accuracy of the optical model. The excellent agreement between experimental and simulated results shows that the variation of the EL emission due to the capping layer can be entirely accounted for by a change in optical interference effects. The complex interplay between wide-angle and multiple-beam interference can be controlled via the optical thickness of the dielectric capping layer on top of the cathode. Consequently, these interference effects can be exploited to tune the spectral characteristics and the angular intensity distribution as well as to improve light outcoupling. By using this approach we were able to enhance the outcoupled light intensity in forward direction by a factor of 1.7 with high color purity. Furthermore, our investigations have revealed that the dielectric-layer thickness can be used to tailor the angular dependence and that an almost angle-independent spectral characteristic can be achieved.

We have demonstrated that in top-emitting devices the concept of dielectric capping is a powerful tool to improve OLED performance without modifying the electrical properties. In addition we have shown that precise predictions of the emission characteristics of planar OLEDs can be made from numerical simulations. These two breakthroughs are, especially from a technological point of view, of great importance.

ACKNOWLEDGMENTS

The authors are grateful to S. Alvarado, B. Ruhstaller, D. Gundlach, P. Müller and C. Rost for useful discussions, and to M. Tschudy for preparing the substrates. They also thank P. F. Seidler for his continuous support.

[1] C. W. Tang, S. A. Van Slyke, and C. H. Chen, J. Appl. Phys. **65**, 3610 (1989).
[2] J. Kido and T. Matsumoto, Appl. Phys. Lett. **73**, 2866 (1998).
[3] M. A. Baldo, S. Lamansky, P. E. Burrows, M. E. Thompson, and S. R. Forrest, Appl. Phys. Lett. **75**, 4 (1999).
[4] X. Zhou, M. Pfeiffer, J. Blochwitz, A. Werner, A. Nollau, T. Fritz, and K. Leo, Appl. Phys. Lett. **78**, 410 (2001).
[5] C. W. Tang and S. A. Van Slyke, Appl. Phys. Lett. **51**, 913 (1987).
[6] L. S. Hung, C. W. Tang, and M. G. Mason, Appl. Phys. Lett. **70**, 152 (1997).
[7] J. Kido and Y. Iizumi, Appl. Phys. Lett. **73**, 2721 (1998); T. Wakimoto, S. Kawami, K. Nagayama, Y. Yonemoto, R. Murayama, J. Funaki, H. Sato, H. Nakada, and K. Imai, Technical Digest International Symposium on Inorganic and Organic Electroluminescence, Hamamatsu, Japan, October 1994, p. 77; T. Iwakuma, T. Aragane, Y. Hironaka, K. Fukuoka, H. Ikada, C. Hosokawa, and T. Kusumoto, Proc. Soc. Inf. Display **XXXIII**, 598 (2002); C. Hosokawa, S. Toshio, K. Fukuoka, H. Tokailin, Y. Hironaka, H. Ikeda, M. Funahashi, and T. Kusumoto, *ibid.* **XXXIII**, 522 (2001).
[8] T. Tsutsui, M-J. Yang, M. Yahiro, K. Nakamura, T. Watanabe, T. Tsuji, Y. Fukuda, T. Wakimoto, and S. Miyaguchi, Jpn. J. Appl. Phys., Part 2 **38**, L1502 (1999).
[9] M. Ikai, S. Tokito, Y. Sakamoto, T. Suzuki, and Y. Taga, Appl. Phys. Lett. **79**, 156 (2001).
[10] C. F. Madigan, M. H. Lu, and J. C. Sturm, Appl. Phys. Lett. **76**, 1650 (2000).
[11] T. Tsutsui, M. Yahiro, H. Yokogawa, K. Kawano, and M. Yokoyama, Adv. Mater. (Weinheim, Ger.) **13**, 1149 (2001).
[12] S. K. So, W. K. Choi, L. M. Leung, and K. Neyts, Appl. Phys. Lett. **74**, 1939 (1999).
[13] Y. Fukuda, T. Watanabe, T. Wakimoto, S. Miyaguchi, and M. Tsuchida, Synth. Met. **111–112**, 1 (2000).
[14] T. A. Beierlein, H.-P. Ott, H. Hofmann, H. Riel, B. Ruhstaller, B. Crone, S. Karg, and W. Rieß, Proc. SPIE **4464**, 178 (2002).
[15] K. Neyts, P. De Visschere, D. K. Fork, and G. B. Anderson, J. Opt. Soc. Am. B **17**, 114 (2000).
[16] A. Vasicek, *Optics of Thin Films* (North-Holland, Amsterdam, 1960).
[17] L. S. Hung, C. W. Tang, M. G. Mason, P. Raychaudhuri, and J. Madathil, Appl. Phys. Lett. **78**, 544 (2001).
[18] K. Neyts, J. Opt. Soc. Am. A **15**, 962 (1998).
[19] H. Riel *et al.* (unpublished).
[20] H. Riel, T. Beierlein, S. Karg, and W. Rieß, Proceedings of 11th International Workshop on Inorganic and Organic Electroluminescence–EL2002, Ghent, Belgium, September 2002, p. 317.
[21] H. Riel, S. Karg, T. Beierlein, B. Ruhstaller, and W. Rieß, Appl. Phys. Lett. **82**, 466 (2003).
[22] W. Lukosz, J. Opt. Soc. Am. **71**, 744 (1981).
[23] K. Neyts, in *Semiconductors and Semimetals* (Academic, New York, 2000), Vol. 65, p. 183.
[24] F. De Martini, M. Marrocco, P. Mataloni, L. Crescentini, and R. Loudon, Phys. Rev. A **43**, 2480 (1991).
[25] V. Bulović, V. B. Khalfin, G. Gu, and P. E. Burrows, Phys. Rev. B **58**, 3730 (1998).
[26] M.-H. Lu and J. C. Sturm, J. Appl. Phys. **91**, 595 (2002).
[27] K. B. Kahen, Appl. Phys. Lett. **78**, 1649 (2001).
[28] *Handbook of Chemistry and Physics* (CRC Press, Boca Raton, FL, 1996).
[29] T. Tsutsui and K. Yamamato, Jpn. J. Appl. Phys., Part 1 **38**, 2799 (1999).
[30] H. Becker, S. E. Burns, N. Tessler, and R. H. Friend, J. Appl. Phys. **81**, 2825 (1997).